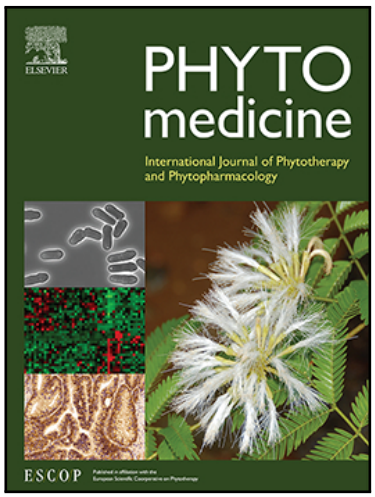

Cnicin promotes functional nerve regeneration

Philipp Gobrecht , Jeannette Gebel , Marco Leibinger , Charlotte Zeitler , Zhendong Chen , Dirk Gründemann , Dietmar Fischer

PII: S0944-7113(24)00300-3
DOI: https://doi.org/10.1016/j.phymed.2024.155641
Reference: PHYMED 155641

To appear in: *Phytomedicine*

Received date: 19 December 2023
Revised date: 24 March 2024
Accepted date: 13 April 2024

Please cite this article as: Philipp Gobrecht , Jeannette Gebel , Marco Leibinger , Charlotte Zeitler , Zhendong Chen , Dirk Gründemann , Dietmar Fischer , Cnicin promotes functional nerve regeneration, *Phytomedicine* (2024), doi: https://doi.org/10.1016/j.phymed.2024.155641

Cnicin promotes functional nerve regeneration

Philipp Gobrecht, Jeannette Gebel, Marco Leibinger, Charlotte Zeitler, Zhendong Chen, Dirk Gründemann and Dietmar Fischer

Center of Pharmacology, Institute for Pharmacology, Medical Faculty and University of Cologne, Paul-Schallück-Straße 8, 50937, Cologne, Germany

Correspondence and proofs:

Dietmar Fischer, Ph.D.

Center of Pharmacology

Medical Faculty and University of Cologne

Paul-Schallück-Straße 10

50937, Cologne, Germany

Email: dietmar.fischer@uni-koeln.de

Tel.: +49 15165757791

Acknowledgments: We thank Anastasia Andreadaki, Simone Kalis, Samira Boussettaoui, and Kessy Brzozowski for their technical support. The Federal Ministry of Education and Research supported this work.

Abbreviations

BDNF: brain-derived neurotrophic factor

CNS: central nervous system

CNTF: ciliary neurotrophic factor

DMSO: dimethyl sulfoxide

GFP: green fluorescent protein

LC-MS: liquid chromatography-mass spectrometry

NGF: nerve growth factor

PNS: peripheral nervous system

SNC: sciatic nerve crush

SSI: static sciatic index

STAT3: signal transducer and activator of transcription 3

JAK: Janus Kinase

SVBP: small vasohibin binding protein

VASH1/2: vasohibin 1/2

Abstract

Backround: The limited regenerative capacity of injured axons hinders functional recovery after nerve injury. Although no drugs are currently available in the clinic to accelerate axon regeneration, recent studies show the potential of vasohibin inhibition by parthenolide, produced in *Tanacetum parthenium,* to accelerate axon regeneration. However, due to its poor oral bioavailability, parthenolide is limited to parenteral administration. **Purpose:** This study investigates another sesquiterpene lactone, cnicin, produced in *Cnicus benedictus* for promoting axon regeneration. **Results:** Cnicin is equally potent and effective in facilitating nerve regeneration. In culture, cnicin promotes axon growth of sensory and CNS neurons from various species, including humans. Neuronal overexpression of vasohibin increases the effective concentrations comparable to parthenolide, suggesting an interaction between cnicin and vasohibin. Remarkably, intravenous administration of cnicin significantly accelerates functional recovery after severe nerve injury in various species, including the anastomosis of severed nerves. Pharmacokinetic analysis of intravenously applied cnicin shows a blood half-life of 12.7 minutes and an oral bioavailability of 84.7% in rats. Oral drug administration promotes axon regeneration and recovery after nerve injury in mice. **Conclusion:** These results highlight the potential of cnicin as a promising drug to treat axonal insults and improve recovery.

Key words: axon regeneration, cnicin, sesquiterpene lactone, nerve injury

Introduction

Although injured axons in the peripheral nervous system (PNS) usually have a remarkable regenerative capacity, complete functional recovery is often elusive. This is because Schwann cells cease providing growth-promoting support after about 3 months, and axons exit their growth state (Barnes et al., 2022; Hoke, 2006; Scheib and Hoke, 2013; Sulaiman and Gordon, 2013). At a maximum rate of 1-2 mm per day, regenerating axons can, therefore, typically only cover distances of approximately 9-18 cm (Sulaiman and Gordon, 2013; Sunderland, 1947). If reinnervation does not occur within this time frame, the injury often results in lifelong incomplete recovery and the formation of neuromas, which can contribute to the development of neuropathic pain (Grinsell and Keating, 2014). For these reasons, there is a great need for treatment strategies that allow accelerated axon growth to facilitate or improve recovery (Daeschler et al., 2023; Diekmann and Fischer, 2016; Faroni et al., 2015; Grinsell and Keating, 2014). Although proteins, such as nerve growth factor (NGF) and brain-derived neurotrophic factor (BDNF), enhance axon growth in mice, their clinical value in humans is limited due to severe side effects (Diekmann and Fischer, 2016; Faroni et al., 2015; Grinsell and Keating, 2014). The immunosuppressant tacrolimus has also been reported to stimulate axon regeneration when used in conjunction with autologous nerve grafts (Faroni et al., 2015). However, the prolonged administration of tacrolimus required for long-distance axon growth in humans results in decreased bone stability and induction of hypertension, which also limits its clinical applicability (Grinsell and Keating, 2014). Therefore, surgery can only treat injured nerves according to their severity.

A critical factor influencing the axon growth rate is the dynamics of microtubule (MT) filaments in axonal growth cones (Chakraborti et al., 2016). They regulate various cellular processes such as shape determination, division, motility, and cell differentiation (Gadadhar et al., 2017). Microtubules are cylindrical structures formed through the dynamic assembly of αβ-tubulin heterodimers that are highly conserved throughout evolution. The C-termini of the α- and β-tubulin subunits are exposed on the outer surface of the microtubule and exhibit variations in length and amino acid sequence among different tubulin isotypes (Gadadhar et

al., 2017; Janke, 2014). Within axons, microtubules are primarily organized with their β-tubulin facing toward the axonal tip (known as the plus end) and the α-tubulin oriented toward the cell body (referred to as the minus end) (Chakraborti et al., 2016). The rate at which tubulin dimers are added to the plus-end of microtubules depends on various post-translational modifications of the α-tubulin subunit (Sanyal et al., 2023), with particular emphasis on the C-terminal detyrosination (Baas and Black, 1990). αβ-tubulin heterodimers exhibit a higher rate of addition to the plus end than the minus end, thereby propelling the growth cone forward (Fukushima et al., 2009). Interestingly, the tips of extending axons carry a high proportion of tyrosinated MT (Ahmad et al., 1993; Baas and Black, 1990; Brown et al., 1993; Shea, 1999). Tubulin detyrosination is achieved by the action of the carboxypeptidases vasohibin 1 (VASH1) and vasohibin 2 (VASH2), the specific enzymes responsible for this process (Aillaud et al., 2017; Gobrecht et al., 2024; Nieuwenhuis et al., 2017). These enzymes have been proposed to be regulated by calpain 1 and 2 (Bär et al., 2022). VASHs can be pharmacologically inhibited by the sesquiterpene lactone parthenolide leading to reduced microtubule detyrosination (Aillaud et al., 2017; Freund et al., 2020; Li et al., 2019). The partial inhibition of each VASH by knockdown or parthenolide significantly promotes axon growth of cultured adult sensory neurons or retinal ganglion cells (Gobrecht et al., 2024; Leibinger et al., 2023). At 1000-fold higher concentrations, parthenolide also reportedly blocks tubulin detyrosination by forming adducts on both cysteine and histidine residues on tubulin itself, thereby preventing the formation of microtubules in HeLa cells (Hotta et al., 2021). However, its low oral bioavailability significantly restricts its efficacy as a treatment for peripheral nerve injury (Gobrecht et al., 2024; Leibinger et al., 2023).

Parthenolide has an αMγB structure. This structure binds covalently to the 169Cys residue within the catalytic Cys-His-Ser triad of VASH1 through a sulfa-Michael addition. This interaction was determined by co-crystallizing a truncated VASH1 (comprising the catalytic domain, spanning residues 52 to 310), small vasohibin binding protein (SVBP), and the natural compound parthenolide (Li et al., 2019). In this binding context, the oxygen atom within parthenolide's epoxide group forms a hydrogen bond with a nearby serine residue.

Additionally, parthenolide engages in several hydrophobic interactions with surrounding amino acid residues (Li et al., 2019).

In this manner, parthenolide blocks the catalytic center of VASH, thereby inhibiting tubulin detyrosination. However, while an intravenous administration of parthenolide improved sciatic nerve regeneration in mice and rats, orally applied parthenolide was ineffective due to its poor oral bioavailability (Gobrecht et al., 2024; Guzman et al., 2007). Thus, *Tanacetum parthenium* extracts containing parthenolide cannot be used orally. Because oral bioavailable drugs are advantageous, especially for long-term use, we searched for structurally similar compounds that could similarly interact with VASH1/2 and be used to promote axon regeneration and functional recovery. One potential candidate was the sesquiterpene-dihydroxyacetone cnicin (Vanhaelen-Fastre, 1972), which, as parthenolide, reportedly reduces microtubule detyrosination in HeLA cells (Fonrose et al., 2007). While parthenolide and cnicin have similar core structures, they differ in the size of their rings and the functional groups attached to them. Whereas parthenolide's structure includes a seven-membered ring with an epoxide group and an alpha-methylene gamma-lactone moiety, cnicin contains a gamma-lactone moiety but has a five-membered ring. Additionally, cnicin lacks the epoxy group postulated as essential for the binding to VASH (Li et al., 2019). Cnicin is found in the plant *Cnicus benedictus*, commonly known as the blessed thistle (Vanhaelen-Fastre, 1972). However, compared to parthenolide, relatively little is known about cnicin, and no pharmacokinetic data are available.

The current study demonstrates that cnicin is as potent as parthenolide in inhibiting microtubule detyrosination in axonal tips and promoting axon growth of rat, mouse, and rabbit sensory neurons in culture. Moreover, intravenous application of the compound (2 µg/kg) significantly accelerates axon growth and functional recovery after severe nerve injury in several species, including anastomosis of the transected nerve. We also investigated the pharmacokinetic parameters of cnicin and demonstrated that daily repeated oral treatments fully mimic the beneficial effects of the intravenously applied cnicin, making cnicin a promising candidate for drug development for treating axonal nerve insults.

Material and Methods

Surgical procedures

All animal protocols conformed to animal care guidelines and were approved by the local authorities (LANUV Recklinghausen). Male and female adult (8-12 weeks) C57/BL6J mice, Lewis rats, and male New Zealand rabbits were maintained in cages of 1-5 animals on a 12 h light/dark cycle with *ad libitum* access to food and water. Sciatic nerve crush (SNC) was performed as previously described (Gobrecht et al., 2016; Gobrecht et al., 2014). In brief, animals were anesthetized with 2% isoflurane in oxygen, and a skin incision of ~10 mm was made above the gluteal region. The ischiocrural musculature was then carefully spread with minimal tissue damage to expose the right sciatic nerve from the sciatic notch to the point of trifurcation. Crush injury was performed proximal to the tibial and peroneal divisions using graphite powder-dipped Dumont #5 forceps (Hermle) to mark the crush site. To ensure a standardized crush, the tip of the forceps was fully squeezed together for 10 seconds. After crushing, the skin was then closed with 6-0 sutures. After the surgery, animals received daily intravenous or oral indicated doses of cnicin (phytolab) or parthenolide (Merck) in 100 µl vehicle (dimethyl sulfoxide, DMSO).

Quantification of regenerating axons in the sciatic nerve

Sciatic nerves were isolated 3 d after SNC, postfixed in 4% paraformaldehyde (PFA) overnight, dehydrated in 30% sucrose at 4°C again overnight, and embedded in Tissue-Tek (Sakura). Longitudinal sections (14 µm) were cut on a cryostat (Leica), thawed onto coated glass slides (Superfrost Plus, Fisher), and stored at -20°C. Cryosections were immunohistochemically stained with antibodies against the regeneration-associated sensory axon marker superior cervical ganglia 10 protein (SCG10; 1:1000; Novus Biologicals, RRID:AB_10011569) (Shin et al., 2012), the motor axon marker choline acetyltransferase (ChAT; 1:100; Sigma, RRID:AB_90661) or the sympathetic axon marker tyrosine hydroxylase (TH, 1:500; Novus Biologicals, RRID:AB_10077691). In addition, labeled axons beyond the graphite-labeled injury site were quantified as previously described (Gobrecht et

al., 2016; Gobrecht et al., 2014). Experimental groups comprised four to five animals, and five sections were analyzed per animal. Statistical significance of intergroup differences was evaluated using two- or three-way ANOVA followed by the Holm-Sidak *post hoc* test.

Static sciatic index (SSI)

The static sciatic index (SSI) was determined as described (Baptista et al., 2007; Bobinski et al., 2011; Gobrecht et al., 2014): After SNC, motor recovery was determined by calculating the SSI, as previously described (Gobrecht et al., 2014). At the same time of day (11:00 a.m. - 2:00 p.m.) at different time points after SNC (mice: 0, 1, 4, 7, 9, 14, 21, and 28 d; rats: 0, 1, 7, 9, 11, 14, 16, 18, 21, 24, 28, 30, 32, 35, 37, 42, 45, 49, 53 and 63 d), mice or rats were lifted off the ground to photograph the left and right hind paws, respectively. The treatment was blinded to the experimenter during the experiment. Toe spreading on the contralateral (C, left) and the ipsilateral (I, right) sides relative to the SNC was assessed by measuring paw length (PL) and the distance between the first and fifth toes (FF). The SSI was then calculated using the previously described formula: SSI = 101.3 ((IFF − CFF)/CFF) − 54.03((IPL - CPL)/CPL) - 9.5 (Baptista et al., 2007). Data represent mean ± SEM per experimental group. Statistical significance of intergroup differences were evaluated by two-way ANOVA followed by the Holm-Sidak *post hoc* test.

Von Frey test

The von Frey test was determined as described recently (Gladman et al., 2012; Gobrecht et al., 2016; Gobrecht et al., 2014): Sensory recovery after SNC and MNC was determined at different time points (mice, SNC: 0, 1, 4, 7, 9, 14, 21, 28 d; rats, SNC: 0, 1, 7, 9, 11, 14, 16, 18, 21, 24, 28, 30, 32, 35, 37, 42, 45, 49, 53 and 56 d) after SNC using the von Frey filament test as previously described. The same experimenter, unaware of the treatment, performed tests at the same time of day. Mice or rats were placed on an elevated metal grid (pore size: 2 mm) and allowed to acclimate for 15 min before testing. Starting with the smallest, differently sized, innocuous von Frey filaments (Muromachi Kikai) were consecutively poked

into the ipsilateral hind paw to evoke a paw withdrawal. Statistical significance of intergroup differences was evaluated using two-way ANOVA followed by the Holm-Sidak *post hoc* test.

Analysis of muscle reinnervation after SNC

The treatment with cnicin or vehicle and the SNC was performed as described above. Animals were sacrificed 10 d after SNC. The musculus *extensor hallucis longus* was dissected, fixed in 4% PFA for 1 h, and permeabilized in 2% Triton-X/PBS for 1 h. The tissue was blocked in 2% BSA+ 10% donkey serum. Axons were labeled with an antibody against heavy and medium chain neurofilaments (1:2000; Cell signaling, RRID:AB_10694081) and Alexa488-conjugated secondary antibody. Restored synapses in neuromuscular endplates were visualized by incubation with Alexa594-conjugated α-BTX (1:1000; Invitrogen) for 1 h at room temperature. Representative pictures of each experimental group were captured on an SP8 confocal microscope (Leica).

Analysis of skin reinnervation after SNC

The treatment with cnicin or vehicle and the SNC was performed as described above. Animals were sacrificed 10 days after SNC. The footpads innervated by the sciatic nerve were isolated. Tissue was fixed in 4% PFA at 4°C overnight and dehydrated in 30% sucrose at 4 °C again overnight. 20 µm cryosections were permeabilized in methanol and blocked (2% BSA, 5% donkey serum). Axons were identified by immunostaining against βIII-tubulin (1:1000, BioLegend, RRID:AB_2564645) overnight, and antibodies were detected with anti-rabbit antibodies conjugated with Alexa-594. In addition, nuclei were counterstained with DAPI (Merck).

Axons in the *stratum spinosum* were counted in 25 sections per mouse. Six mice were analyzed per condition. The experimental conditions were blinded for the experimenter. Statistical significance of intergroup differences was evaluated using two-way ANOVA followed by the Holm-Sidak *post hoc* test.

Sensory neuron cultures and immunocytochemical staining

Sensory neurons were obtained from adult mice or rat dorsal root ganglia (DRG). Briefly, isolated DRG were incubated with 0.25% trypsin/EDTA (GE Healthcare) and 0.3% collagenase type IA (Sigma) in DMEM (Invitrogen) at 37°C for 45 min and mechanically dissociated. Cells were resuspended in DMEM containing 2% (v/v) B27 (Thermo Fisher) and penicillin/streptomycin (500 U/ml; Merck, Millipore) and cultured at 37°C and 5% CO_2 on poly-d-lysine (PDL, 0.1 mg/ml, molecular weight <300 kDa; Sigma) and laminin (20 µg/ml; Sigma)-coated 8-well plates (Sarstedt). Cells were treated with vehicle (DMSO) or 0.5-50 nM cnicin. Baculoviral transduction of sensory neurons was achieved as described previously (Levin et al., 2016). In brief, 10 % (v/v) virus solution with a titer of ~10^8 pfu/ml was added to the culture 2 h after plating. Baculoviruses expressed either VASH1 or VASH2, or GFP as a control. After 48 h, the cells were fixed with 4% PFA (Sigma). All fixed cell cultures were subjected to immunocytochemical staining with antibodies against βIII-tubulin (1:1000; BioLegend, RRID:AB_2313773). Imaging was performed automatically with the Olympus VS210-S5 slide scanner. The total axon length was quantified automatically with the NeuriteTracer plugin for ImageJ to avoid experimenter-induced quantification bias. Average axon length per neuron from three wells per condition and neuron counts per experimental group were normalized to control groups. Data represent the mean ± SEM of three independent experiments. Significance of intergroup differences was evaluated using two-way ANOVA followed by the Holm-Sidak *post hoc* test.

Microtubule detyrosination in axon tips was assessed using antibodies against βIII-tubulin (1:1000; BioLegend, RRID:AB_2313773) and detyrosinated tubulin (1:500; Sigma, RRID:mAB_477583) as previously described (Freund et al., 2019a; Freund et al., 2019b). In brief, axon tips were defined as the distal 15 µm of βIII-tubulin-positive neurite extensions. The intensity of detyrosinated tubulin staining in the axon tip was measured using ImageJ, and the adjacent background intensity was subtracted. Intensities were normalized to the respective control group. Data represent mean ± SEM of three replicate wells with 30-60 tips

per well from three independent experiments. The significance of intergroup differences was evaluated using two-way ANOVA followed by the Holm-Sidak *post hoc* test.

Dissociated mouse retinal cell cultures

Adult C57BL/6 mice were used for all cell culture experiments. Retinal cultures were prepared as described previously (Grozdanov et al., 2010). In brief, retinae were dissected from the eyecups and digested in Dulbecco's modified Eagle's medium (DMEM; Thermo Fisher) containing papain (10 U/ml; Worthington) and L-cysteine (0.2 µg/ml; Sigma) at 37°C for 30 min.. After digestion, retinae were washed with DMEM, triturated, and centrifuged in 50 ml DMEM (500 g, 7 min.). Cell pellets were resuspended in a medium containing 2% (v/v) B27 (Thermo Fisher) and penicillin/streptomycin (500 U/ml; Merck, Millipore)and passed through a cell strainer (40 µm; Greiner Bio-One). Cells were treated with cnicin (0.25-5.0 nM in DMSO), recombinant rat CNTF (Peprotech; 200 ng/ml), DMAPT (Abcam; 0.25-5.0 nM in dimethyl sulfoxide), or a combination of cnicin and CNTF. 300 µl cell suspension was added to each well on 4-well plates (Nunc), which were coated with poly-D-lysine (0.1 mg/ml, molecular weight 70,000-150,000 Da; Sigma) and laminin (20 µg/ml; Sigma). Retinal cells were cultured at 37 °C and 5% CO_2.

After 4 days in culture, retinal cells were fixed with 4% paraformaldehyde (PFA; Sigma). Cells were stained with primary antibodies against βIII-tubulin (1:2000; BioLegend, RRID:AB_2313773), detyrosinated tubulin (1:2000; Millipore), and phosphorylated (Tyr705) STAT3 (1:200; Cell Signaling Technology, RRID:AB_2491009). Secondary antibodies included donkey-anti-mouse, and anti-rabbit antibodies conjugated to Alexa Fluor 488 or 594 (1:1000; ThermoFisher).

To examine neurite growth, all RGC neurites were photographed under a fluorescence microscope (200x; Axio Observer.D1, Zeiss), and neurite length was determined using ImageJ software. To evaluate microtubule detyrosination, at least 30 axon tips per well were photographed (400x; Axio Observer.D1, Zeiss) and analyzed using ImageJ software. Axon tips were defined as the last 15 µm of βIII-tubulin-positive neurites. For the quantification of

STAT3 phosphorylation, at least 30 RGCs per well were evaluated (400x; Axio Observer.D1, Zeiss).

Human eyes

The use of human eyes and the publication of the results obtained were approved by the ethics committee of Heinrich Heine University Düsseldorf, Germany (study number 4067) and were conducted in accordance with the ethical standards of the 1964 Declaration of Helsinki and its subsequent amendments or comparable ethical standards.

Dissociated human retinal cell cultures

Primary human retinal cultures were prepared in two independent experiments with retinae isolated from the human eyes of two adult patients.

The retinae were dissected from the eyecups, and the vitreous body was removed. Afterward, the retinae were cut into 8 pieces and digested separately, each in 10 ml DMEM (Thermo Fisher) containing papain (10 U/ml; Worthington) and L-cysteine (0.2 µg/ml; Sigma) at 37°C for 45 min.. After digestion, retinae were washed with DMEM, triturated, and centrifuged in 50 ml DMEM (900 g, 5 min.). Cell pellets were resuspended in a medium containing B27 supplement (1:50; Invitrogen) and penicillin/streptomycin (1:50; Merck) and passed through a cell strainer (40 µm; Greiner Bio-One). Retinal cultures were incubated with cnicin (0.25-5.0 nM in DMSO) or the vehicle. Some groups received recombinant rat CNTF (Peprotech; 200 ng/ml), either alone or combined with cnicin. Cells were cultured at 37 °C and 5% CO_2 on 4-well plates (Nunc) (300 µl/well; 4 wells/group), which were coated with poly-D-lysine (0.1 mg/ml, molecular weight 70,000-150,000 Da; Sigma). After 4 days in culture, retinal cells were fixed with 4% paraformaldehyde (PFA; Sigma) and stained with primary antibodies against βIII-tubulin (1:2000; BioLegend) and detyrosinated tubulin (1:2000; Millipore). Secondary antibodies included donkey-anti-mouse, and anti-rabbit antibodies conjugated to Alexa Fluor 488 or 594 (1:1000; ThermoFisher). Cultures were

analyzed in the same way as described above for murine RGCs to examine neurite growth and the percentage of detyrosinated axon tips.

Quantification of cnicin by LC/MS-MS

Plasma samples were diluted 1:10 with methanol; after centrifugation (5 min, 14,000 g, 4 °C), the supernatant was transferred to glass vials (70213, Macherey-Nagel, Düren, Germany) with insert (702968.1). 20 µl of each sample was injected (autosampler temperature 8 °C) into a SLC-20AD Prominence HPLC system (Shimadzu, Duisburg, Germany) with an Atlantis dC18 column (5 µm, 3 mm x 100 mm; Waters, Dublin, Ireland). A binary gradient (flow rate 0.3 ml/min; oven temperature 40°C) with 0.1% formic acid in water (A) and 0.1% formic acid in methanol (B) was applied as follows: 10% B at 0 min, 97% B at 2 min, 97% B at 4 min, 97% B at 5 min, 10% B at 7 min, and 10% B at 9 min. A triple quadrupole mass spectrometer (4000 QTRAP, AB Sciex, Darmstadt, Germany) analyzed the eluate in positive ion mode with an electrospray ionization (ESI) source. The optimal collision energy for nitrogen-induced fragmentation in the second quadrupole was determined for each analyte. For quantification by selected reaction monitoring (SRM; capillary voltage 5.5 kV, scan time 150 ms), the following fragmentations were selected from the product ion spectra (m/z parent, m/z fragment, collision energy): cnicin, 379, 229, 11 V. For each analyte, the area of the intensity versus time peak was integrated. Linear calibration curves were constructed (weighting $1/y^2$) from at least six standards in diluted control plasma. Sample analyte content was calculated from the analyte peak area and the slope of the calibration curve.

Preparation and collection of cnicin plasma samples

To determine the cnicin plasma concentration after intravenous and oral administration, adult C57/BL6J mice (approximately 25 g) or Lewis rats (approximately 300 g) received intravenous injections of oral gavage applications of 80 µg (mice) or 800 µg (rats) cnicin. At various time points, as indicated, 250 µl blood was collected in a tube containing 96 mg citric

acid and 0.4 mg tripotassium ethylenediaminetetraacetic acid (K_3EDTA). The blood was then centrifuged at 4 °C for 10 min at 1,800 g and 100 µl plasma was collected and stored at -80 °C until LC/MS-MS measurements.

Pharmacokinetic analysis

A population pharmacokinetic model was developed and fit using the nonlinear mixed-effects modeling software NONMEM (version 7.4.0, ICON Development Solutions, USA) and Perl-speaks-NONMEM (PsN, version 5.3.0, Uppsala University, Sweden) (Boeckman et al., 2001; Lindbom et al., 2005). First-order conditional estimation with interaction was used, where a decrease of >3.84 in the objective function value between 2 nested models ($P < 0.05$) upon the inclusion of a parameter was applied as a statistical criterion to select a more complex model (Boeckman et al., 2001). An exponential equation described inter-individual variability for pharmacokinetic parameters, and different residual error models were evaluated. Diagnosis of the final model was performed by individual plots of predicted and observed concentrations and goodness-of-fit (GOF) plots (Suppl. Fig. 2).

Results

Cnicin promotes axon growth and inhibits microtubule detyrosination of sensory neurons

Since parthenolide's insufficient oral bioavailability significantly limits its efficacy in treating peripheral nerve injury, we tested other sesquiterpene lactones, such as cnicin, for potential axon growth-promoting effects. Although lacking the epoxy group of parthenolide, which is thought to be relevant for VASH 1/2 binding (Li et al., 2019), cnicin significantly facilitated axon growth of adult sensory neurons from mice in a similar concentration range as parthenolide (Leibinger et al., 2023) (Fig. 1 A, B). GFP-expressing murine sensory neurons exposed to 0.5 nM cnicin showed the most robust axon growth. In contrast, 5 nM was less effective, and 50 nM even compromised axon growth (Fig. 1 A-B), suggesting that a defined equilibrium range of tyrosinated and detyrosinated microtubules is required for optimal growth. This optimal range corresponded to 60-70% of axon tips positively stained for detyrosinated tubulin (detyr^{+}) in our assay (Fig. 1 C, D). Consistently, 50 nM cnicin reduced the levels of detyrosination in axon tips below 60% (Fig. 1 C, D). In contrast, overexpression of either VASH1 or VASH2 in adult sensory neurons (Fig. 1 E, F), as expected, increased microtubule detyrosination in axonal tips to almost 100% (Fig. 1 D) and significantly reduced axon growth compared to GFP-expressing controls (Fig. 1 B). Cnicin also reduced the detyrosination rate to 60%-70% in these VASH-overexpressing neurons and promoted axon growth. However, at least ten times higher concentrations (5 nM) were required to achieve the effect of 0.5 nM cnicin in GFP-transfected cells, while 0.5 nM remained ineffective with VASH overexpression (Fig. 1 B). Even concentrations of 50 nM, which reduced axon growth in GFP-expressing controls without affecting survival (Suppl. Fig. 1 A), still slightly promoted axon growth in VASH1- or VASH2- overexpressing cells (Fig. 1 B), suggesting that cnicin counteracts the effect of VASH proteins or their effects on microtubules, respectively (Fig. 1 D).

Cnicin promotes axon growth of sensory neurons in different species and CNS neurons.

We next examined whether cnicin also affects axon growth in rats and rabbits sensory neurons. Again, cnicin significantly promoted axon growth in a concentration-dependent manner without affecting neuronal survival (Fig. 2 A, B, E, F; Suppl. Fig. 1 B, C). Moreover, active drug concentrations were similar in all species and showed a bell-shaped curve with cnicin-reducing microtubule detyrosination (Fig. 2 C, D, G, H).

To address whether the drug is sufficient to promote the regeneration of CNS neurons, we cultured retinal ganglion cells (RGC) from adult mice or humans (isolated from enucleated human eyes). As in sensory neurons, cnicin increased the average length of extended neurites with a maximal effect at 0.5 nM in murine (Fig. 3 A, B) and human (Fig. 3 J, K) RGC without affecting the neuronal survival (Fig. 3 C, E; Suppl. Fig. 1 D). Combined with CNTF, a cytokine that promotes neurite growth via JAK/STAT3 activation (Leibinger et al., 2013), these effects were increased synergistically in mouse and human RGCs (Fig. 3 A, D, J, K). While CNTF expectedly induced STAT3 phosphorylation without affecting microtubule detyrosination, cnicin did not impact the JAK/STAT3 pathway but expectedly reduced microtubule detyrosination in mouse and human RGC (Fig. 3 F-G, L, M). Thus, because they affect different mechanisms, cnicin and cytokines synergistically promote the neurite growth of neurons.

Intravenous application of cnicin promotes nerve regeneration.

Next, we conducted tests to determine whether the systemic application of cnicin can promote axon regeneration *in vivo* after sciatic nerve crush (SNC). To this end, we performed the injury and applied daily either vehicle (PBS) or different doses of cnicin into adult mice's tail veins, starting immediately after the injury. Three days later, axon regeneration of superior cervical ganglion-10-positive ($SCG10^+$) sensory neurons, choline acetyltransferase-positive ($CHAT^+$) motoneurons, and tyrosine hydroxylase-positive (TH^+) sympathetic neurons was evaluated in immunostained longitudinal sciatic nerve sections

(Fig. 4 A-H). While low doses of cnicin (0.28 µg/kg) showed a slightly improved axon regeneration of sensory neurons, results were more substantial at 2.8 µg/kg (Fig. 4 A, B). At a higher daily dose of 28 µg/kg, the beneficial effect of cnicin diminished again (Fig. 4 A, B), thus correlating with the bell-shaped curve observed in cell culture (Fig. 1 A, B). Intravenous treatment with cnicin (2.8 µg/kg) increased all three neuronal subpopulations' axonal lengths compared to the respective vehicle-treated control groups (Fig. 4 A-H). TH^+-axons were the longest among these different fiber types. They extended up to 5 mm beyond the lesion site at this early time point after injury, indicating a higher rate of axonal regeneration in sympathetic neurons than in sensory or motor neurons (Fig. 4 E-H).

Systemic cnicin accelerates sensory and motor recovery

We then investigated whether intravenous administration of cnicin can accelerate clinically relevant functional recovery after SNC injury. To this end, we evaluated motor and sensory function using the static sciatic index (SSI) and the von Frey test, respectively, over 4 weeks after injury (Gobrecht et al., 2014). Strikingly, daily repeated doses of the compound (2.8 µg/kg) significantly improved the SSI score and touch sensitivity compared to vehicle-treated controls (Fig. 4 I-K). Furthermore, the onset of incipient functional motor recovery and the achievement of full recovery were significantly accelerated by cnicin administration (Fig. 4 I-K). Remarkably, in contrast to vehicle-treated controls, cnicin-treated mice showed the first measurable improvements in motor function as early as 4 d after injury (Fig. 4 I, J). Treatment effects of cnicin concerning the touch response (von Frey) were detectable 7 d after injury (Fig. 4 K). Moreover, cnicin was similarly effective in promoting motor and sensory recovery as previously reported for parthenolide (Fig. 4 I-K,). At the same time, systemically applied cnicin significantly enhanced skin and muscle reinnervation 10 days after SNC (Fig. 4 L-O). Strikingly, oral application of cnicin also accelerated functional recovery with the same efficacy as intravenous injection, while oral parthenolide had no effect (Fig. 4 P-R) due to its poor oral bioavailability.

Pharmacokinetics and oral bioavailability of Cnicin

Pharmacokinetic data on cnicin in mammals were not available. Therefore, we investigated its profile after intravenous and oral administration. Due to the low recoverable blood volume of mice, we first investigated the pharmacokinetic parameters in rats and developed a method to measure cnicin plasma levels using high-performance liquid chromatography-mass spectrometry (LC-MS), which allows a detection limit of 5 µM (Fig. 5 A). Then, Wistar rats (300 g) received a single intravenous injection of 800 µg cnicin, and plasma samples were collected up to 120 min later (Fig. 5 B). Peak plasma concentrations of 133.8 ± 25.8 µM were observed 2 min after injection, while cnicin was undetectable after 60 min. To investigate cnicin's bioavailability, the same dose (800 µg) was administered orally. In this case, peak plasma concentrations reached 29.5 ± 9.3 µM and were approximately 6 times lower than after intravenous application. Joint data analysis of the intravenous and peroral administration using a population pharmacokinetic approach showed that the concentration-time profiles of cnicin were best described by a two-compartment model with first-order elimination and an additive residual error model. The GOF plots showed no obvious bias in the model fit. The parameter estimates of the final model are provided in Table 1. The central volume of distribution of cnicin was 10.6 mL, corresponding to the plasma volume of rats (300 g) (Lee and Blaufox, 1985). Cnicin apparent terminal elimination half-life, calculated from parameter point estimates for the terminal (β) slope of the concentration vs. time curve via microconstants, was about 12.7 min (Gabrielsson and Hjorth, 2016). The absolute bioavailability for oral administration of cnicin was high, reaching 84.7% (point estimate). This is consistent with similar pharmacodynamic effects following both intravenous and oral administration.

Since cnicin has a short plasma half-life, we next investigated possible elimination pathways by incubating blood, plasma, and PBS with equimolar amounts of cnicin at 37°C. Cnicin concentrations were quantified after up to 120 min (Fig. 5 C). While the compound showed only a slow decay in plasma or PBS, its concentrations decreased at a similar rate as in the *in vivo* bloodstream when incubated in whole blood, suggesting that cnicin is either taken up

by, bound to, or is metabolized in blood cells. We, therefore, explored the formation of metabolites in these samples. Interestingly, as the concentration of cnicin in PBS decreased, the concentration of cnicin with an open γ-butyrolactone ring increased simultaneously (Fig. 5 D), suggesting a slow degradation in plasma and PBS by hydrolytic opening of the γ-butyrolactone ring. We then investigated whether orally applied cnicin is also detectable in the serum of mice. Because of the small blood volume, we determined the concentrations only 2, 30, and 120 min after oral gavage application. Consistent with the rat data, orally applied cnicin was detectable 30 min after application in quantities similar to those in rat plasma (Fig. 5 E).

Cnicin accelerates functional nerve recovery in rats and rabbits

To determine the efficacy of cnicin in species that require to overcome longer regeneration distances to recover, adult rats received daily doses of either vehicle or cnicin (0.2, 2, and 20 µg/kg/d) intravenously, beginning immediately after SNC. While 0.2 µg/kg/d showed only a slight but non-significant effect on motor recovery, efficacy was, like in mice, stronger and significant at the higher doses (Fig. 6 A-B). The first effects on motor recovery were evident at 14 d after injury (Fig. 6 B), whereas these were seen in vehicle-treated rats at 21 d. Moreover, cnicin-treated rats reached pre-injury SSI scores after 35 d. In comparison, the control group required another 7 d to reach these levels (Fig. 6 A, B). Sensory recovery was likewise accelerated by intravenous cnicin treatment (Fig. 6 C), with daily doses of 2 µg/kg showing the strongest effects. In this group, improvements in touch sensation were first seen in this group after 21 d, and reached pre-surgery levels after 35 d. In comparison, the vehicle group needed 49 d (Fig. 6 C). All groups reached the same level of hypersensitivity after 49 d (Fig. 6 C), which is generally observed in rats.

From a clinical perspective, it is important to know whether a delay in treatment or only a few days of initial treatment is still sufficient to promote axon regeneration. Therefore, we examined four groups where 2 µg/kg of cnicin was intravenously administered daily using different treatment regimes. Rats of group 1 received a vehicle for 28 d; rats of group 2

received a vehicle for the first 5 d and then cnicin for the remaining 23 d; animals of group 3 received cnicin for the first 5 d and then the vehicle for the remaining 23 d; rats of group 4 received cnicin daily for the entire 28 d. As expected, continuous cnicin treatment (group 4) showed the fastest motor and sensory recovery, whereas group 1 (vehicle only) was the slowest (Fig. 6 D-F). Moreover, animals of group 2 with a postponed treatment showed a slower functional improvement (Fig. 6 D-F) but only a slightly weaker effect at later time points than group 4. Finally, animals of group 3, treated for the initial 5 d only, showed similar initial improvement as group 4 but were less effective than group 2 at later time points (Fig. 6 D-F). Thus, although continuous cnicin treatment over the entire period showed the best results, a delayed treatment was still effective.

Finally, to demonstrate the efficacy of cnicin in promoting sciatic nerve recovery beyond rodents, we extended our investigation to rabbits. To this end, we crushed the sciatic nerves of adult rabbits and treated them daily with various intravenous cnicin doses or a vehicle (Fig. 7 A, B). After 4 days, the axon growth into the sciatic nerve was determined. While low doses of cnicin (0.2 µg/kg) did not improve axon regeneration, 2 µg/kg significantly increased axon growth into the sciatic nerve. Higher daily doses of 20 µg/kg abolished the beneficial effect of cnicin (Fig. 7 A, B), thus correlating with the bell-shaped curve observed in mice and rats (Fig. 4, 6).

Discussion

Peripheral nerves have the intrinsic ability to regenerate damaged axons; however, achieving practical and functionally significant restoration often proves challenging due to the limited axon growth rate. Given the high clinical demand for effective treatments, accelerating axon regeneration has been a central focus of nerve regeneration research for decades. In a recent study, we demonstrated that the sesquiterpene lactone parthenolide significantly accelerates axon regeneration in both adult CNS and PNS neurons after intravenous administration through the covalent inhibition of vasohibin (VASH) (Gobrecht et al., 2016; Gobrecht et al., 2024; Marco Leibinger, 2023). VASH inhibition leads to a reduction in microtubule detyrosination and an increase in microtubule dynamics within the axonal growth cone. However, due to its limited bioavailability parthenolide cannot be administered orally (Leibinger et al., 2023).

In the current study, we have now demonstrated that a structurally analogous compound, cnicin, which lacks an epoxy group compared to parthenolide, exhibits similar properties in enhancing axonal growth in cell culture and promoting functional nerve recovery across various species. Given the structural similarity between cnicin and parthenolide, it is likely that these effects are also mediated through covalent VASH inhibition. This finding is intriguing because it contradicts the conventional understanding that the epoxy group in parthenolide, which is replaced by an ethanol group in cnicin, was considered indispensable for binding to VASH (Li et al., 2019). This implies that the ethanol group in cnicin may be a satisfactory substitute for enzyme binding instead of the epoxy group. Notably, previous investigations have shown that cnicin can inhibit microtubule detyrosination in a cell line, albeit at concentrations over 20,000 times higher (Fonrose et al., 2007). While we cannot completely dismiss the possibility that cnicin's regenerative effects are mediated by an alternative and yet undiscovered mechanism distinct from VASH inhibition, this scenario seems unlikely. This is substantiated by cnicin inhibiting microtubule detyrosination and compensates for the reduced axon growth resulting from VASH overexpression when administered at higher concentrations (Fig. 1 A, B). Furthermore, the effective concentration

range of cnicin (Gobrecht et al., 2024) closely aligns with that of parthenolide. To unequivocally confirm the binding of cnicin to VASH, further investigations, such as X-ray structure analysis or alternative enzymatic binding assays, would be required.

In addition to the absence of the potentially mutagenic epoxy group, another distinct advantage of cnicin over parthenolide is its high bioavailability of 84.7%, as shown in the current study. This has been proven directly via the quantification of cnicin in blood samples and functionally by the acceleration of functional regeneration after oral cnicin application. Cnicin has a shorter apparent terminal elimination half-life than previously measured for parthenolide (cnicin: 12.7 min; parthenolide: 73 min) (Zhao et al., 2016). Nevertheless, this relatively short apparent terminal elimination constant of cnicin in the blood seems to be sufficient to reach axonal growth cones, the presumed site of action, and then interact with the respective VASH proteins. This also suggests that cnicin covalently binds to the active site of VASHs, irreversibly inhibiting these proteins and thus causing the persisting effect. Moreover, the effect of higher doses on axonal regeneration is again reduced, reflecting the situation in cell culture that excessive inactivation of VASHs is unfavorable for regeneration. Therefore, optimizing the application regimen may enhance the effect on nerve regeneration additionally. In particular, multiple doses distributed throughout the day and less than 2 µg/kg/day could be considered.

The short blood half-life of cnicin suggests that it is caused by the binding of cnicin to blood cells, as cnicin disappears from the plasma of blood circulating in the rat and isolated rat blood at comparable rates (Fig. 5 C). In contrast, the amount of cnicin in isolated rat plasma, i.e., without the presence of the hematocytes, decreases much more slowly. Therefore, cnicin is likely eliminated from rat blood by binding to hematocytes. Interestingly, this result was observed at doses 1000 times higher than the therapeutic dose. This suggests that therapeutic doses of cnicin do not saturate in hematocytes. Again, these conclusions support the notion that more frequent cnicin applications may further enhance the PNS's axonal regeneration.

Furthermore, even a delayed onset of cnicin application was sufficient to accelerate functional recovery. This is interesting since patients with peripheral nerve injury, e.g., from trauma, often suffer from various other complications that need to be addressed before the nerve injury itself can be treated. In addition, since regeneration distances in humans tend to be greater, this aspect may be particularly relevant to patients.

Compared to parthenolide, another notable advantage of cnicin as a potential therapeutic agent for peripheral nervous system (PNS) injury is its readily accessible extraction process. Although a synthetic pathway for cnicin has not been established to date, it can be obtained through a straightforward ethanol extraction procedure from the Blessed Thistle plant (Horn, 2018). This distinctive feature makes cnicin the first naturally occurring, orally bioavailable compound known to have a regenerative effect on axonal regrowth within the PNS. However, Blessed Thistle plant extractions or teas cannot be readily employed for the treatment of nerve injuries. This is due to the relatively narrow therapeutic window of the axon growth-promoting effect of cnicin, wherein its efficacy diminishes or vanishes entirely upon overdose. Consequently, only extracts containing meticulously adjusted quantities of cnicin are suitable for therapeutic purposes. This necessity underscores the imperative for future studies to investigate the stability of cnicin and determine optimal doses for human application before considering its therapeutic use.

While Cnicin possesses a therapeutic window, toxic effects did not even appear far above therapeutic doses. We performed toxicity tests in 6 rats, which received daily either 2 mg/kg (1000x the therapeutic dose) or 4 mg/kg (2000x the therapeutic dose) of Cnicin intravenous for 14 consecutive days. These doses were well tolerated without any signs of toxicity or changes in body weight.

In conclusion, the current study underscores the potential of cnicin as a readily administered oral compound for augmenting axonal regeneration. It demonstrates a substantial *in vivo* and *in vitro* impact across multiple species, including an effect on cultured primary human nerve cells, even at remarkably low dosages. Consequently, cnicin is a promising candidate for further drug development to treat nerve damage and promote regeneration.

Literature

Ahmad, F.J., Pienkowski, T.P., Baas, P.W., 1993. Regional differences in microtubule dynamics in the axon. J Neurosci 13, 856-866.

Aillaud, C., Bosc, C., Peris, L., Bosson, A., Heemeryck, P., Van Dijk, J., Le Friec, J., Boulan, B., Vossier, F., Sanman, L.E., Syed, S., Amara, N., Coute, Y., Lafanechere, L., Denarier, E., Delphin, C., Pelletier, L., Humbert, S., Bogyo, M., Andrieux, A., Rogowski, K., Moutin, M.J., 2017. Vasohibins/SVBP are tubulin carboxypeptidases (TCPs) that regulate neuron differentiation. Science 358, 1448-1453.

Baas, P.W., Black, M.M., 1990. Individual microtubules in the axon consist of domains that differ in both composition and stability. J Cell Biol 111, 495-509.

Baptista, A.F., Gomes, J.R., Oliveira, J.T., Santos, S.M., Vannier-Santos, M.A., Martinez, A.M., 2007. A new approach to assess function after sciatic nerve lesion in the mouse - adaptation of the sciatic static index. J Neurosci Methods 161, 259-264.

Bär, J., Popp, Y., Koudelka, T., Tholey, A., Mikhaylova, M., 2022. Regulation of microtubule detyrosination by Ca2+ and conventional calpains. J Cell Sci 135.

Barnes, S.L., Miller, T.A., Simon, N.G., 2022. Traumatic peripheral nerve injuries: diagnosis and management. Curr Opin Neurol 35, 718-727.

Bobinski, F., Martins, D.F., Bratti, T., Mazzardo-Martins, L., Winkelmann-Duarte, E.C., Guglielmo, L.G., Santos, A.R., 2011. Neuroprotective and neuroregenerative effects of low-intensity aerobic exercise on sciatic nerve crush injury in mice. Neuroscience 194, 337-348.

Brown, A., Li, Y., Slaughter, T., Black, M.M., 1993. Composite microtubules of the axon: quantitative analysis of tyrosinated and acetylated tubulin along individual axonal microtubules. J Cell Sci 104 (Pt 2), 339-352.

Chakraborti, S., Natarajan, K., Curiel, J., Janke, C., Liu, J., 2016. The emerging role of the tubulin code: From the tubulin molecule to neuronal function and disease. Cytoskeleton (Hoboken) 73, 521-550.

Daeschler, S.C., Feinberg, K., Harhaus, L., Kneser, U., Gordon, T., Borschel, G.H., 2023. Advancing Nerve Regeneration: Translational Perspectives of Tacrolimus (FK506). Int J Mol Sci 24.

Diekmann, H., Fischer, D., 2016. Parthenolide: a novel pharmacological approach to promote nerve regeneration. Neural Regen Res 11, 1566-1567.

Faroni, A., Mobasseri, S.A., Kingham, P.J., Reid, A.J., 2015. Peripheral nerve regeneration: experimental strategies and future perspectives. Adv Drug Deliv Rev 82-83, 160-167.

Fonrose, X., Ausseil, F., Soleilhac, E., Masson, V., David, B., Pouny, I., Cintrat, J.C., Rousseau, B., Barette, C., Massiot, G., Lafanechere, L., 2007. Parthenolide inhibits tubulin carboxypeptidase activity. Cancer Res 67, 3371-3378.

Freund, R.R.A., Gobrecht, P., Fischer, D., Arndt, H.D., 2020. Advances in chemistry and bioactivity of parthenolide. Nat Prod Rep 37, 541-565.

Freund, R.R.A., Gobrecht, P., Moser, P., Fischer, D., Arndt, H.D., 2019a. Synthesis and biological profiling of parthenolide ether analogs. Org Biomol Chem 17, 9703-9707.

Freund, R.R.A., Gobrecht, P., Rao, Z., Gerstmeier, J., Schlosser, R., Gorls, H., Werz, O., Fischer, D., Arndt, H.D., 2019b. Stereoselective total synthesis of parthenolides indicates target selectivity for tubulin carboxypeptidase activity. Chem Sci 10, 7358-7364.

Fukushima, N., Furuta, D., Hidaka, Y., Moriyama, R., Tsujiuchi, T., 2009. Post-translational modifications of tubulin in the nervous system. J Neurochem 109, 683-693.

Gabrielsson, J., Hjorth, S., 2016. Pattern Recognition in Pharmacodynamic Data Analysis. AAPS J 18, 64-91.

Gadadhar, S., Bodakuntla, S., Natarajan, K., Janke, C., 2017. The tubulin code at a glance. J Cell Sci 130, 1347-1353.

Gladman, S.J., Huang, W., Lim, S.-N., Dyall, S.C., Boddy, S., Kang, J.X., Knight, M.M., Priestley, J.V., Michael-Titus, A.T., 2012. Improved outcome after peripheral nerve injury in mice with increased levels of endogenous omega-3 polyunsaturated fatty acids. Journal of Neuroscience 32, 563-571.

Gobrecht, P., Andreadaki, A., Diekmann, H., Heskamp, A., Leibinger, M., Fischer, D., 2016. Promotion of Functional Nerve Regeneration by Inhibition of Microtubule Detyrosination. J Neurosci 36, 3890-3902.

Gobrecht, P., Gebel, J., Hilla, A., Gisselmann, G., Fischer, D., 2024. Targeting vasohibins to promote axon regeneration. The Journal of Neuroscience, e2031232024.

Gobrecht, P., Leibinger, M., Andreadaki, A., Fischer, D., 2014. Sustained GSK3 activity markedly facilitates nerve regeneration. Nat Commun 5, 4561.

Grinsell, D., Keating, C.P., 2014. Peripheral nerve reconstruction after injury: a review of clinical and experimental therapies. Biomed Res Int 2014, 698256.

Grozdanov, V., Muller, A., Sengottuvel, V., Leibinger, M., Fischer, D., 2010. A method for preparing primary retinal cell cultures for evaluating the neuroprotective and neuritogenic effect of factors on axotomized mature CNS neurons. Curr Protoc Neurosci Chapter 3, Unit3 22.

Guzman, M.L., Rossi, R.M., Neelakantan, S., Li, X., Corbett, C.A., Hassane, D.C., Becker, M.W., Bennett, J.M., Sullivan, E., Lachowicz, J.L., Vaughan, A., Sweeney, C.J., Matthews, W., Carroll, M., Liesveld, J.L., Crooks, P.A., Jordan, C.T., 2007. An orally bioavailable parthenolide analog selectively eradicates acute myelogenous leukemia stem and progenitor cells. Blood 110, 4427-4435.

Hoke, A., 2006. Mechanisms of Disease: what factors limit the success of peripheral nerve regeneration in humans? Nat Clin Pract Neurol 2, 448-454.

Horn, G., 2018. Benediktenkraut (Cnicus benedictus L.) zur Einschränkung von Durchfallerkrankungen bei Ferkeln, in: Kluge, H. (Ed.).

Hotta, T., Haynes, S.E., Blasius, T.L., Gebbie, M., Eberhardt, E.L., Sept, D., Cianfrocco, M., Verhey, K.J., Nesvizhskii, A.I., Ohi, R., 2021. Parthenolide Destabilizes Microtubules by Covalently Modifying Tubulin. Curr Biol 31, 900-907 e906.

Janke, C., 2014. The tubulin code: molecular components, readout mechanisms, and functions. J Cell Biol 206, 461-472.

Lee, H.B., Blaufox, M.D., 1985. Blood volume in the rat. J Nucl Med 26, 72-76.

Leibinger, M., Andreadaki, A., Diekmann, H., Fischer, D., 2013. Neuronal STAT3 activation is essential for CNTF- and inflammatory stimulation-induced CNS axon regeneration. Cell Death Dis 4, e805.

Leibinger, M., Zeitler, C., Paulat, M., Gobrecht, P., Hilla, A., Andreadaki, A., Guthoff, R., Fischer, D., 2023. Inhibition of microtubule detyrosination by parthenolide facilitates functional CNS axon regeneration. Elife 12.

Levin, E., Diekmann, H., Fischer, D., 2016. Highly efficient transduction of primary adult CNS and PNS neurons. Sci Rep 6, 38928.

Li, F., Hu, Y., Qi, S., Luo, X., Yu, H., 2019. Structural basis of tubulin detyrosination by vasohibins. Nat Struct Mol Biol 26, 583-591.

Marco Leibinger, C.Z., Miriam Paulat, Philipp Gobrecht, Alexander Hilla, Anastasia Andreadaki, Rainer Guthoff, Dietmar Fischer, 2023. Inhibition of microtubule detyrosination by parthenolide facilitates functional CNS axon regeneration, BioRxiv.

Nieuwenhuis, J., Adamopoulos, A., Bleijerveld, O.B., Mazouzi, A., Stickel, E., Celie, P., Altelaar, M., Knipscheer, P., Perrakis, A., Blomen, V.A., 2017. Vasohibins encode tubulin detyrosinating activity. Science 358, 1453-1456.

Sanyal, C., Pietsch, N., Ramirez Rios, S., Peris, L., Carrier, L., Moutin, M.J., 2023. The detyrosination/re-tyrosination cycle of tubulin and its role and dysfunction in neurons and cardiomyocytes. Semin Cell Dev Biol 137, 46-62.

Scheib, J., Hoke, A., 2013. Advances in peripheral nerve regeneration. Nat Rev Neurol 9, 668-676.

Shea, T.B., 1999. Selective stabilization of microtubules within the proximal region of developing axonal neurites. Brain Res Bull 48, 255-261.

Shin, J.E., Miller, B.R., Babetto, E., Cho, Y., Sasaki, Y., Qayum, S., Russler, E.V., Cavalli, V., Milbrandt, J., DiAntonio, A., 2012. SCG10 is a JNK target in the axonal degeneration pathway. Proc Natl Acad Sci U S A 109, E3696-3705.

Sulaiman, W., Gordon, T., 2013. Neurobiology of peripheral nerve injury, regeneration, and functional recovery: from bench top research to bedside application. Ochsner J 13, 100-108.

Sunderland, S., 1947. Rate of regeneration in human peripheral nerves; analysis of the interval between injury and onset of recovery. Arch Neurol Psychiatry 58, 251-295.

Vanhaelen-Fastre, R., 1972. [Antibiotic and cytotoxic activity of cnicin isolated from Cnicus benedictus L]. J Pharm Belg 27, 683-688.

Zhao, A.Q., Zhao, J.H., Zhang, S.Q., Pan, Y.Y., Huo, X.L., 2016. Determination of parthenolide in rat plasma by UPLC-MS/MS and its application to a pharmacokinetic study. J Pharm Biomed Anal 119, 99-103.

Tables

Table 1: Pharmacokinetic parameters of cnicin following intravenous or oral (n=4 each) administration of 0.8 mg single doses of cnicin in rats

	Final model	
Parameters	Estimate	RSE (%)
K_a (1/min)	0.0321	18.4
CL (L/min)	0.00101	10.7
V_c (L)	0.00745	8.9
F1 (%)	0.847	14.6
Q_p (L/min)	0.00298	5.0
V_p (L)	0.00985	12.5
Lag time (min)	5.02	13.6
Inter-individual variability		
CL (%)	17.2 (13.0)	31.6
V_c (%)	29.0 (32.0)	27.8
Residual variability		
Additive error (cnicin, %)	4.76 (6.4)	12.1

RSE, relative standard error; K_a, apparent absorption constant rate; CL, clearance; V_c, central compartment volume; F1, absolute bioavailability for oral administration; Q_p, inter-compartmental clearance between central and peripheral compartments; V_p, peripheral compartment volume.

Units of PK parameters, shrinkage estimates of IIVs, and residual variabilities are shown in respective parentheses. The additive residual error is expressed as coefficients of variation.

Figure legends

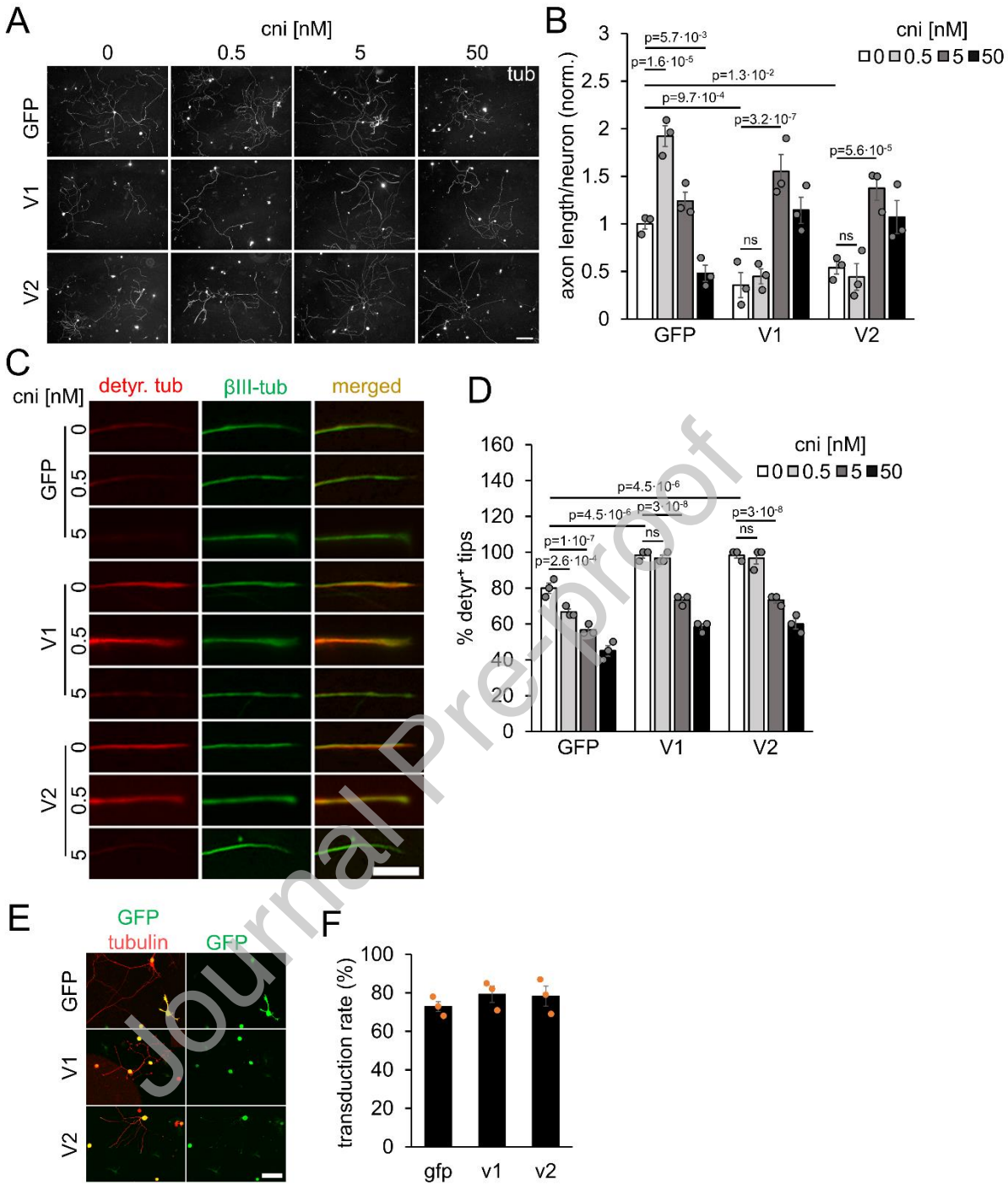

Figure 1: Cnicin promotes sensory neuron axon growth and reduces microtubule detyrosination in axon tips.

A) Representative images of βIII-tubulin-positive (tub) adult murine sensory neurons after 2 d in culture, treated with 0.5, 5, or 50 nM cnicin (cni) or vehicle (DMSO). Additionally, neurons were baculovirally transduced with either GFP, VASH1 (V1), or VASH2 (V2). Scale

bar, 250 µm. **B)** Quantification of axon growth from cultures as depicted in A. Data were normalized to veh-treated GFP controls with an average axon length of 678 µm/neuron. **C)** Sensory neuron cultures, as shown in A, were stained against detyrosinated tubulin (detyr. tub, red) and βIII-tubulin (βIII-tub, green). Scale bar, 5 µm. **D)** Quantification of detyrosinated tubulin-positive axon tips from cultures as described in A. **E)** Representative pictures of adult murine sensory neurons after 2 d in culture, baculovirally transduced with GFP, VASH1 (V1), or VASH2 (V2). Axons were stained for GFP (green) and βIII-tubulin (tubulin, red). Scale bar, 250 µm. **F)** Quantification of the transduction rate of sensory cultures described in E. Transduced neurons were recognized by colocalization of βIII-tubulin and GFP expression, which was co-expressed by the baculovirus. **B, D, F)** Data represents the mean ± SEM of three independent experiments. Dots represent the mean of independent experiments. P-values were determined using two-way ANOVA followed by the Holm-Sidak *post hoc* test. Lines connect bars between which a significant p-value was determined.

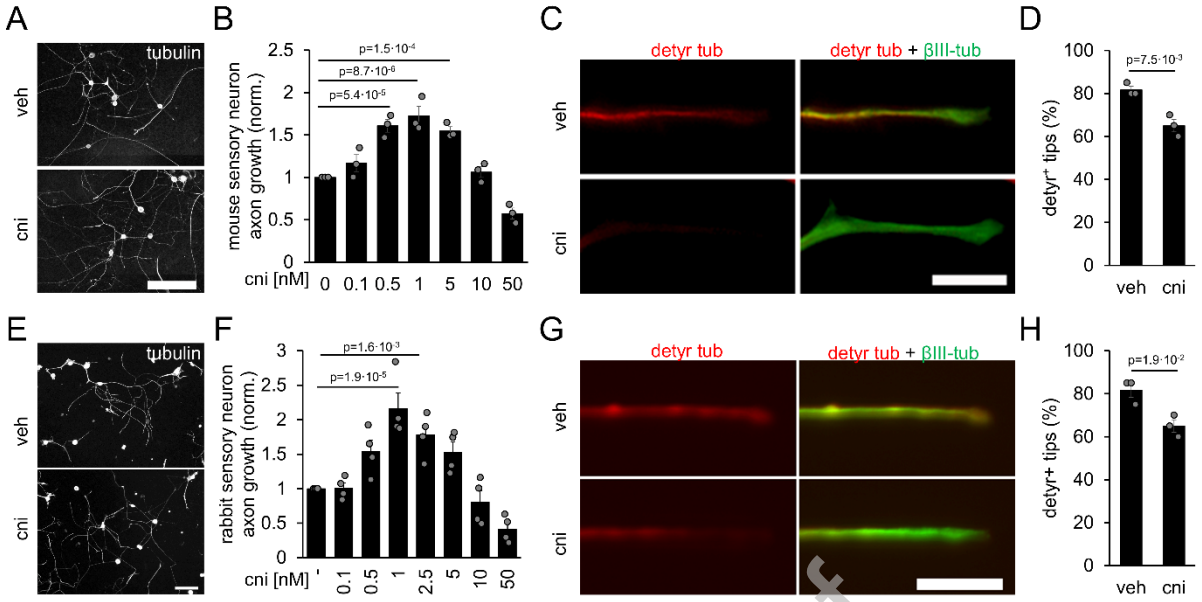

Figure 2: Cnicin promotes axon growth of rat and rabbit sensory neurons.

A) Photos of adult rat sensory neurons after 2 d in culture, treated with 1 nM cnicin or a vehicle. Axons were stained for βIII-tubulin (tub). Scale bar, 250 µm. **B)** Quantification of axon growth from cultures depicted in A and additional ones treated with 0.1, 0.5, 5, 10, or 50 nM cnicin. Data were normalized to vehicle-treated controls with an average axon length of 832 µm/neuron. **C)** Sensory neurons from cultures shown in A stained against detyrosinated tubulin (detyr. tub, red) and βIII-tubulin (βIII-tub, green). Scale bar, 5 µm. **D)** Quantification of detyrosinated tubulin in axon tips of cultures described in C. Data represent the mean ± SEM of three independent experiments, each represented by a dot. P-values were determined by student's T-test. **E)** Photos of adult rabbit sensory neurons after 2 d in culture, treated with 1 nM cnicin or a vehicle. Axons were stained for tub. Scale bar, 250 µm. **F)** Quantification of axon growth from cultures depicted in E and additional ones treated with 0.1, 0.5, 2.5, 5, 10, and 50 nM cnicin. Data were normalized to vehicle-treated controls with an average axon length of 563 µm/neuron. **G)** Sensory neuron cultures shown in E stained against detyrosinated tubulin (detyr. tub, red) and βIII-tubulin (βIII-tub, green). Scale bar, 5 µm. **H)** Quantification of detyrosinated tubulin in axon tips of cultures described in G. Data represent the mean ± SEM of three independent experiments, each represented by a dot. P-values were determined by student's T-test.

B, F) Data represent the mean ± SEM of three independent experiments (n=3). One dot represents each of the three independent experiments. P-values were determined using one-way ANOVA followed by the Holm-Sidak *post hoc* test. The lines connect the bars between which a significant P-value was determined.

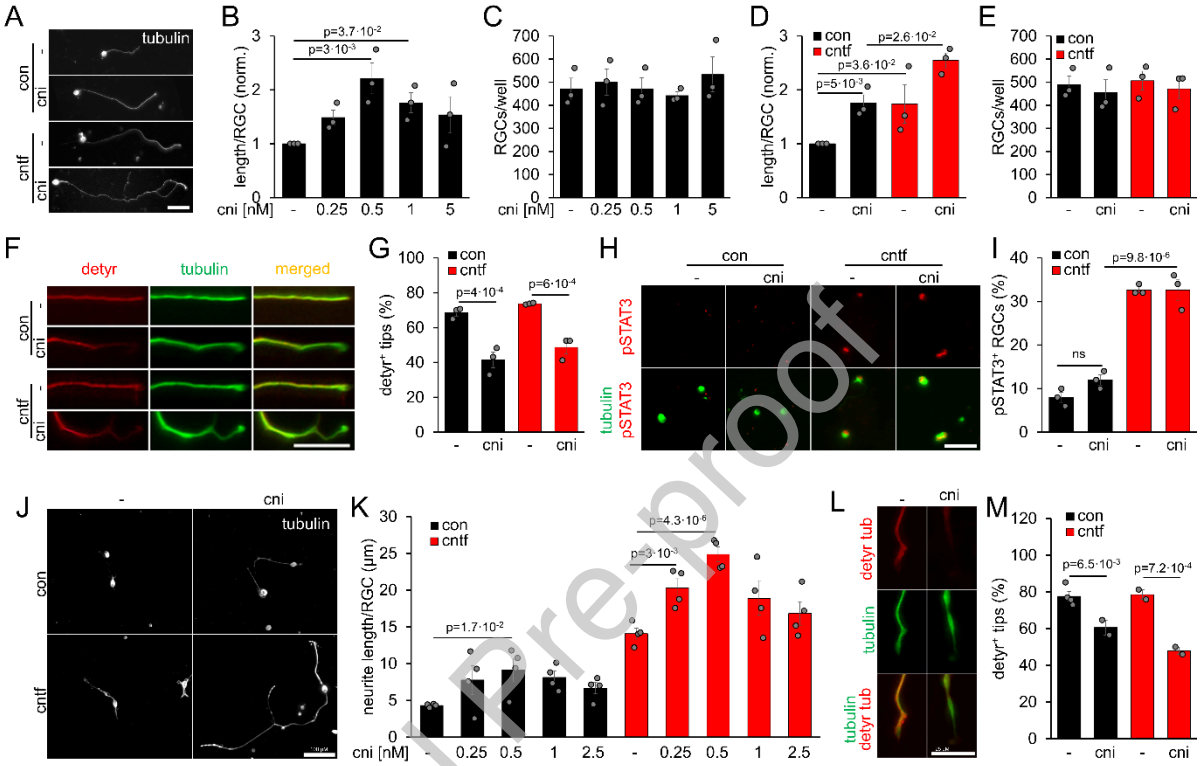

Figure 3: Cnicin promotes neurite growth of murine and human retinal ganglion cells.

A) Adult murine retinal ganglion cells (RGCs) 4 d in culture, treated with 0.5 nM cnicin or a vehicle and cntf or a respective vehicle. Axons were stained for βIII-tubulin (tubulin). Scale bar, 100 µm. **B)** Quantification of axon growth of RGC cultures treated with 0, 0.25, 0.5, 1, and 5 nM cnicin. Data were normalized to vehicle-treated controls with an average axon length of 11.78 µm/neuron. **C)** Quantification of RGC numbers from cultures described in B. Data represent the mean ± SEM of three independent experiments (n=3). **D)** Quantification of axon growth of RGC cultures treated with a vehicle (-) or 0.5 nM cnicin (cni) and/or cntf (bars in red) or a respective control (bars in black, con). **E)** Quantification of RGC numbers from cultures described in D. Data represent the mean ± SEM of three independent experiments (n=3). **F)** Axon tips of RGC neurons from cultures shown in A stained against detyrosinated tubulin (detyr. tub, red) and tubulin (green). Scale bar, 5 µm. **G)** Quantification

of detyrosinated tubulin in axon tips of cultures described in F. **H)** RGC cultures described in A stained against phosphorylated STAT3 (pSTAT3, red) and βIII-tubulin (tubulin, green). Scale bar, 50 µm. **I)** Quantification of pSTAT3 positive RGCs of cultures described in A. **J)** Representative photos of adult human retinal ganglion cells (RGCs) 4 d in culture, treated with 0.5 nM cnicin or a vehicle and cntf or a respective vehicle. Axons were stained for tubulin. Scale bar, 100 µm. **K)** Quantification of axon growth of RGC cultures treated with 0, 0.25, 0.5, 1, and 2.5 nM cnicin and cntf or a respective vehicle. Data was normalized to vehicle-treated controls with an average axon length of 4.31 µm/neuron. Data represents the mean ± SEM of four technical repetitions, each represented by a dot. P-values were determined using two-way ANOVA followed by the Fisher LSD *post hoc* test. The lines connect the bars between which a significant P-value was determined. **L)** Axon tips of RGC neuron cultures shown in J stained against detyr tub (red) and tubulin (green). Scale bar, 5 µm. **M)** Quantification of detyr tub in axon tips of cultures described in L. Data represent the mean ± SEM of 2-4 technical repetitions, each represented by a dot. P-values were determined using two-way ANOVA followed by the Holm-Sidak *post hoc* test. The lines connect the bars between which a significant P-value was determined. **B, D, G, I)** Data represent the mean ± SEM of three independent experiments (n=3). A dot represents each of the three independent experiments. P-values were determined using two-way ANOVA followed by the Holm-Sidak *post hoc* test. The lines connect the bars between which a significant P-value was determined.

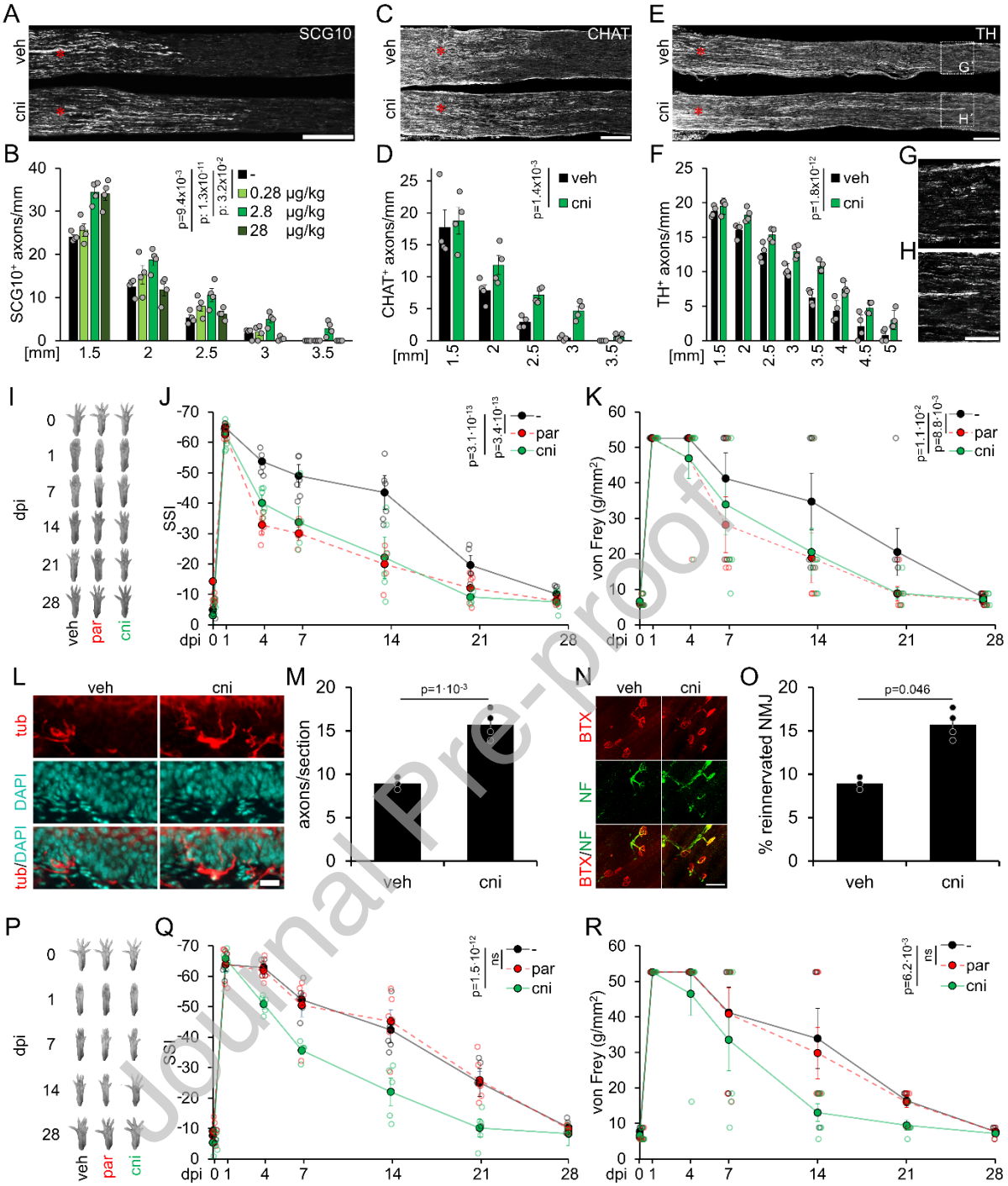

Figure 4: Systemic administration of cnicin accelerates anatomical and functional sciatic nerve regeneration in adult mice

A, C, E) Longitudinal sciatic nerve sections from adult mice 3 days after sciatic nerve crush (SNC). Mice were treated with 2.8 µg/kg cnicin (cni) or a vehicle (veh). Regenerating sensory axons are stained with antibodies against the Superior Cervical Ganglion-10 protein (SCG10) in A, motor axons are stained with antibodies against choline acetyltransferase (CHAT) in C, and sympathetic neurons are stained with antibodies against tyrosine

hydroxylase (TH) in E. Scale bars: 500 µm. **B, D, F)** Quantification of regenerating axons at indicated distances beyond the injury site in the sciatic nerve of mice depicted in A, C, and E. Some mice in B were treated with additional cnicin concentrations, namely 0.28 µg/kg and 28 µg/kg. Data represent the mean ± SEM. Each dot represents four averaged nerve sections from a single animal. P-values were determined by two-way ANOVA followed by the Holm-Sidak *post hoc* test. Statistically significant P-values are compared to the control group (veh). **G, H)** Magnifications of nerve sections indicated in E. Scalebar: 200 µm. **I)** Photos of right hind paws of mice before (0) or 1, 7, 14, 21, and 28 days (dpi) after sciatic nerve crush (SNC). Animals had received daily intravenous doses of either vehicle (-), 2 µg/kg of parthenolide (par), or 2 µg/kg cnicin (cni). **J)** Quantification of motor recovery in mice paws as depicted in I, showing the SSI over 28 d after SNC and daily intravenous injection with vehicle (-), par, or cni. **K)** Quantification of sensory recovery in the same mice described in I and J was determined with the von Frey test. **L)** Representative pictures of epidermal footpad reinnervation 10 days after SNC stained for tub (red) and counterstained with DAPI (cyan). Scale bar 20 µm. **M)** Quantification of data depicted in L. Data represent mean ± SEM (bars) and single values (dots) of three to four individual animals (veh n=3; cni n=4). P-values were determined using student's t-test. **N)** Representative pictures of *musculus extensor hallucis longus* (EHL) isolated 10 dpi and stained for neurofilament (NF; green) and α-bungarotoxin (BTX; red). Scale bar 20 µm. **O)** Quantification of data depicted in N. Data represents mean ± SEM (bars) and single values (dots) of three to four individual animals (veh n=3; cni n=4). P-values were determined by student's t-test. **P)** Photos of right hind paws of mice before (0) or 1, 7, 14, 21, and 28 d (dpi) after sciatic nerve crush (SNC). Animals had received daily oral doses of either vehicle (-), 2 µg/kg of parthenolide (par), or 2 µg/kg cnicin. **Q)** Quantification of motor recovery in the paws of mice as depicted in P, showing the SSI over 28 d after SNC and daily intravenous injection of vehicle (-), par, or cni. **R)** Quantification of sensory recovery in the same mice described in P and Q was determined with the von Frey test. **J, K, Q, R)** Data represent the mean ± SEM of six separate animals (n=6). Each hollow dot represents a single animal. P-values were

determined using two-way ANOVA followed by the Holm-Sidak *post hoc* test. The lines connect the bars between which a significant P-value was determined.

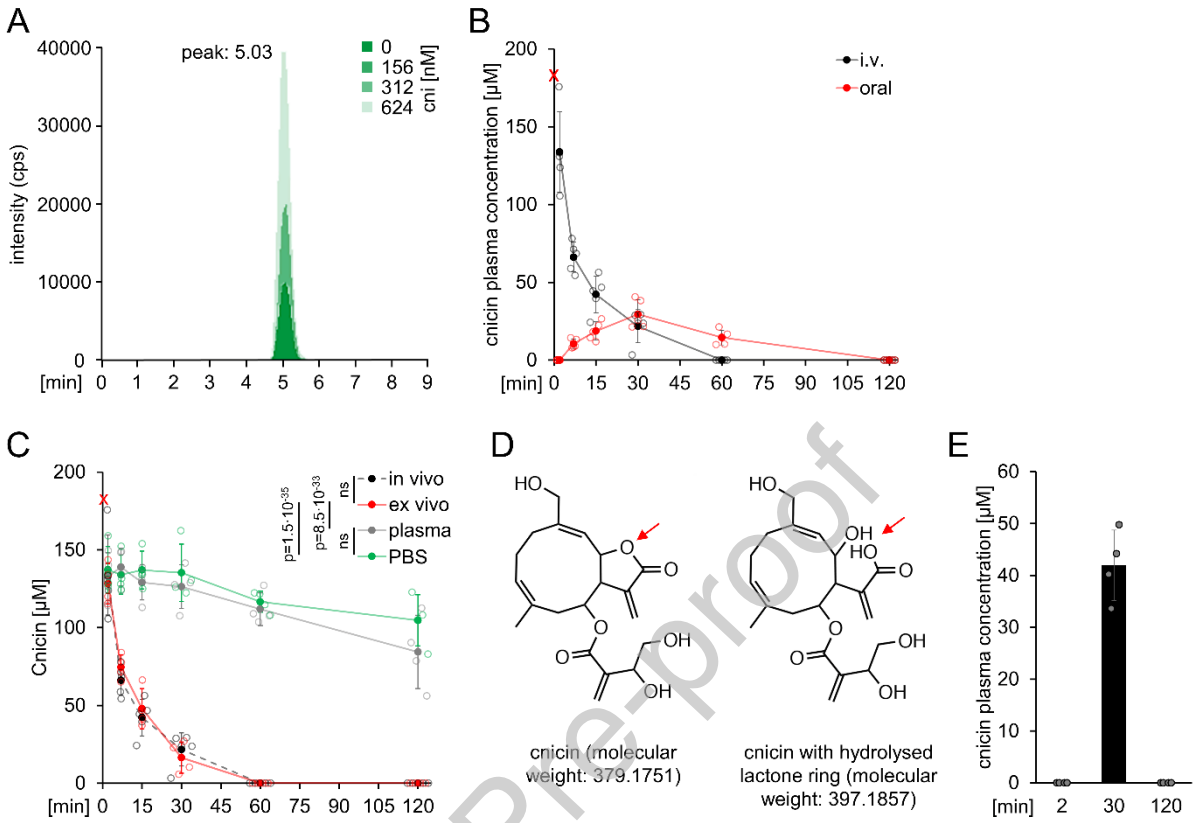

Figure 5: Cnicin is detectable in the rat and mouse plasma after oral administration

A) Cnicin (cni) molecule counts per second of rat plasma samples spiked with cnicin at the indicated concentrations. Counts were determined by HPLC. **B)** Cnicin plasma concentration in rats 2, 7, 15, 30, 60 and 120 min. after intravenous (i.v.) or oral cnicin application (800 µg/rat) determined with HPLC. Data represent mean ± SEM (bars) and single values (dots) of individual animals. **C)** Decrease of cnicin in the blood from rats *in vivo* or *ex vivo*, in rat plasma and in PBS, 2, 7, 15, 30, 60, or 120 min after cnicin application at 37 °C. **D)** Molecular structure of cnicin and a possible degradation product found in PBS 120 minutes after spiking cnicin into the serum. The degradation product had a mass consistent with a hydrolyzed lactone ring. **E)** Cnicin plasma concentration in mice 2, 30, and 120 min**.** after oral cnicin application (80 µg/mouse) determined by HPLC. Data represent mean ± SEM (bars) and single values (dots) of individual animals.

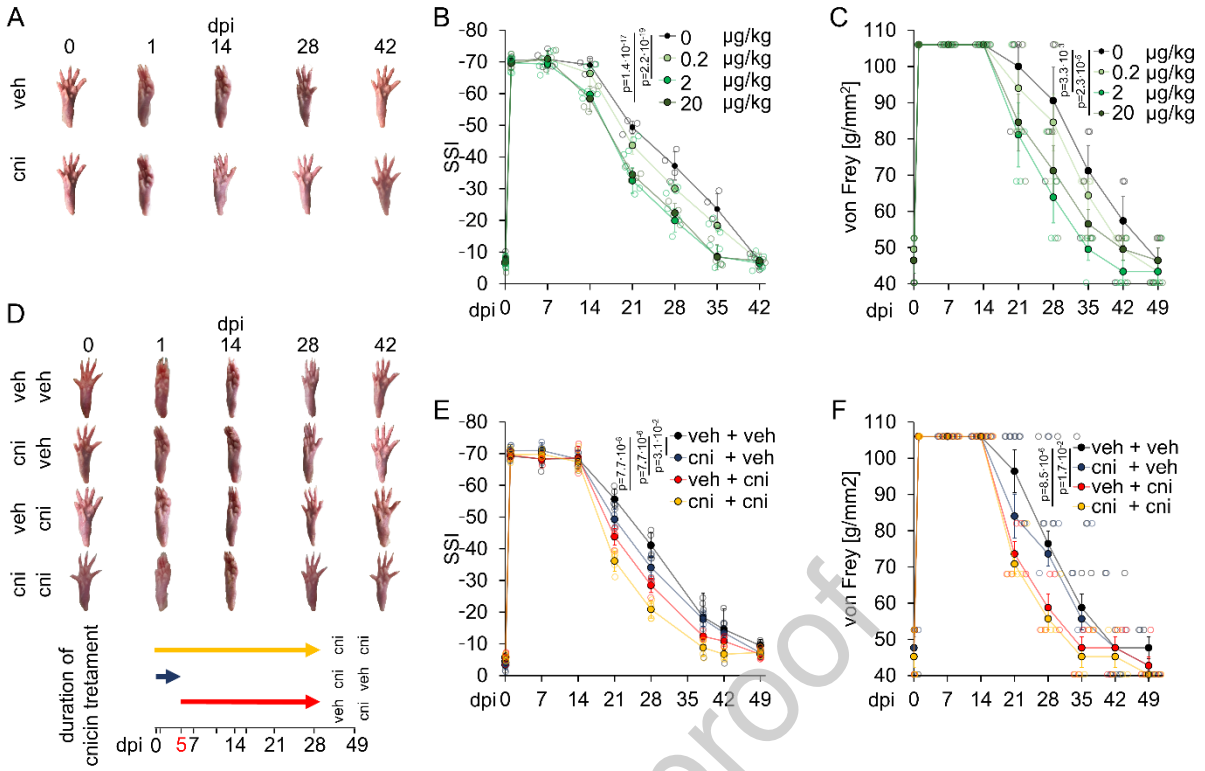

Figure 6: Systemic application of cnicin promotes functional recovery in rats

A) Representative photos of right hind paws of rats before (0) or 1, 14, and 28 d after sciatic nerve crush (SNC; dpi). Adult rats received daily intravenous doses of either vehicle (0) or 2 µg/kg of cnicin (cni). **B)** Quantification of motor recovery in adult rats as depicted in A by the static sciatic index after SNC and daily intravenous injections of different doses of 0.2 µg/kg, 2 µg/kg, or 20 µg/kg cnicin for 49 d. **C)** Quantification of sensory recovery in the same rats described in B determined by the von Frey test. B, C) Data represent the mean ± SEM, each hollow dot an individual animal (n=6). P-values were determined using two-way ANOVA followed by the Holm-Sidak *post hoc* test. Statistical differences were calculated within each timepoint to compare the control (0 µg/kg) and each treatment group. The significant P-values are displayed in the color of the line of the treatment group. **D)** Representative photos of the right hind paw of rats before (0) or 1, 14, and 21 dpi and different treatment regimens. Animals received daily treatment (intravenous injections) of either vehicle (veh) or cnicin (cni) from days 0-5 or 6-28 dpi as indicated. Another group received cnicin treatment from 0-28 dpi. **E)** Quantification of motor recovery in animals as depicted in D by the static sciatic index over 42 dpi. **F)** Quantification of sensory recovery in

the same rats described in D and E determined by the von Frey test. E, F) Data represent the mean ± SEM, each hollow dot an individual animal (n=6). P-values were determined using two-way ANOVA followed by the Holm-Sidak *post hoc* test. Statistical differences were calculated within each timepoint to compare the control (veh veh) and each treatment group. The significant P-values are displayed in the color of the line of the treatment group.

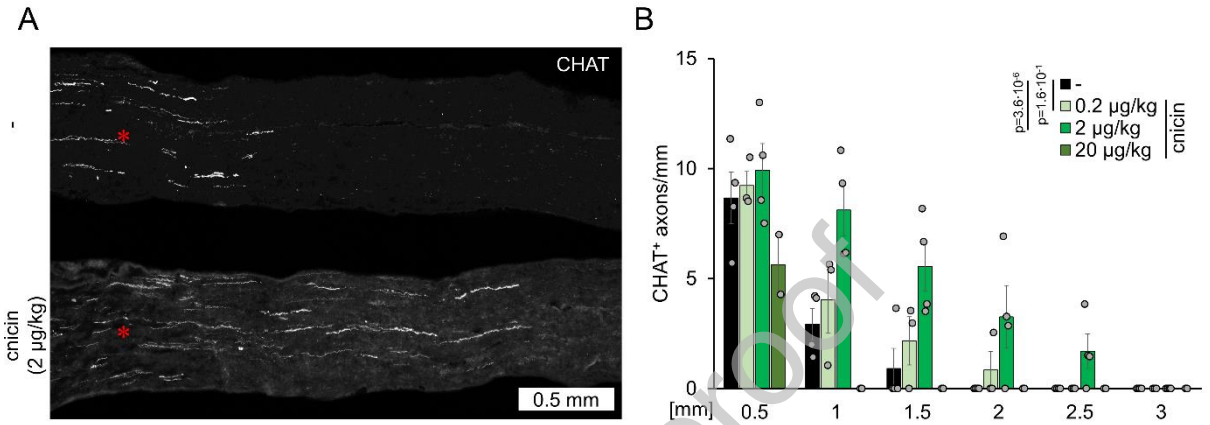

Figure 7: Systemic cnicin application accelerates sciatic nerve regeneration in adult rabbits

A) Longitudinal sciatic nerve sections from adult rabbits 4 days after sciatic nerve crush (SNC). Rabbits were treated with 2 µg/kg cnicin or a vehicle (-). Regenerating motor axons are stained with antibodies against choline acetyltransferase (CHAT). Scale bar: 500 µm. **B)** Quantification of regenerating axons at indicated distances beyond the injury site in the sciatic nerve of rabbits depicted in A. Additional rabbits were treated with different cnicin concentrations, namely 0.2 µg/kg and 2 µg/kg. Data represent the mean ± SEM. Each dot represents four averaged nerve sections from an individual animal. P-values were determined using two-way ANOVA followed by the Holm-Sidak *post hoc* test. Statistically significant P-values are compared with control (veh).

Supplementary Figure 1: Cnicin is not cytotoxic for cultured sensory and retinal ganglion cells.

A) Quantification of adult murine sensory neuron numbers of 2-day cultures transfected with gfp, VASH1 (v1) or VASH2 (v2) and treated with 0, 0.5, 5, and 50 nM cnicin (cni). Data represent the mean ± SEM of three independent experiments (n=3), each represented by a dot. **B)** Quantification of adult murine sensory neuron numbers of 2-day cultures treated with 0, 0.5, 5, and 50 nM cnicin (cni). Data represent the mean ± SEM of three independent experiments (n=3), each represented by a dot. **C)** Quantification of adult rabbit sensory neuron numbers of 2-day cultures treated with 0, 0.5, 5, and 50 nM cnicin (cni). Data represent the mean ± SEM of four independent experiments (n=4), each represented by a dot. **D)** Quantification of adult murine retinal ganglion cells (RGC) numbers of 4-day cultures treated with 0, 0.25, 0.5, 1, and 5 nM cnicin (cni). Data represent the mean ± SEM of four technical replicates (n=4), each represented by a dot.

Supplementary Figure 2: Goodness of fit plots of the model for cnicin plasma concentrations: DV: observed concentrations, CWRES: conditional weighted residuals, TIME: time after dose. The red lines show the local polynomial regression fit.

Graphical Abstract

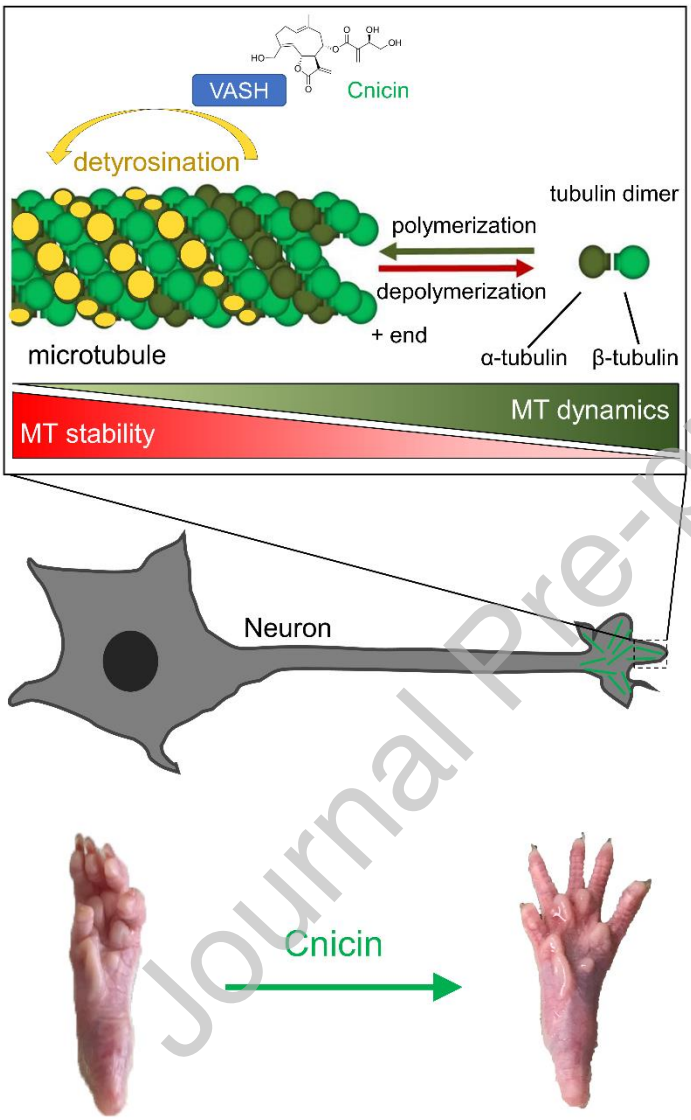

Declaration of interest statement

The authors declare that they have no known competing financial interests or personal relationships that could have appeared to influence the work reported in this article.